Eur. Phys. J. D (2018) 72: 29
https://doi.org/10.1140/epjd/e2017-80422-1

THE EUROPEAN PHYSICAL JOURNAL D

Regular Article

Structure, stability, and electronic and magnetic properties of small Rh_nMn ($n = 1$–12) clusters

Ru Shan, Ling Suo, Jin Lv[a], and Hai-Shun Wu

School of Chemistry and Material Science, Shanxi Normal University, Linfen 041004, P.R. China

Received 20 June 2017 / Received in final form 28 November 2017
Published online 6 February 2018 – © EDP Sciences, Società Italiana di Fisica, Springer-Verlag 2018

Abstract. The structure, stability, and magnetic properties of Rh_{n+1} and Rh_nMn clusters ($n = 1$–12) are systematically investigated within the framework of the generalized gradient approximation density-functional theory (DFT-GGA). The overall structural evolutionary trend shows that the ground state structures of the Rh_nMn are similar to that of the corresponding pure rhodium clusters except for $n = 7$, 9, 12, while the Rh_7Mn, Rh_9Mn and $Rh_{12}Mn$ clusters occur substantially geometry reconstruction. The binding energy of Rh_nMn is decreased with the substitution of one Mn atom, thus indicating that Mn doping can weaken the stability of the Rh clusters. The fragmentation energy and the second-order difference energy of the ground-state Rh_nMn clusters imply that the Rh_3Mn, Rh_5Mn, Rh_8Mn and $Rh_{11}Mn$ clusters are more stable than their neighbors. Compared with corresponding pure Rh_n clusters, the Mn atom doping increases the total magnetic moment of the Rh_nMn clusters in various degrees, and the physics origin of such a phenomenon is analyzed in detail based on the average bond length, magnetic coupling, and density of state.

1 Introduction

Metal clusters have attracted considerable research interest in the past few decades owing to their fundamental importance and potential applications. At the nanoscale, transition metal (TM) clusters exhibit fantastic electronic, optical, magnetic, and catalytic properties due to their small size and large surface to volume ratio. Among the $3d$, $4d$, and $5d$ TM clusters, rhodium clusters have been extensively investigated both experimentally [1,2] and theoretically [3–10] due to the wide range of applications in catalysis. Rhodium clusters are employed as promising catalysts for heterogeneous catalysis, for example in hydrogenation and hydrodechlorination reactions [11–13]. Particularly, Rh is the most efficient catalyst for the catalytic dissociation of NO [14]. In addition, rhodium clusters present special magnetic properties in contrast to the paramagnetic behavior of bulk Rh. Therefore, the development of stable Rh clusters with large magnetic moment has been given much attention.

Although bulk Rh is a nonmagnetic metal, Rh clusters exhibit magnetic moments with n up to 60 at 60–300 K [1,2]. Furthermore, the magnetic moments of small rhodium clusters show strong dependence on size and structure; particularly, Rh_{15}, Rh_{16}, and Rh_{19} clusters possess a large magnetic moment. An experimental study [1] showed that small Rh_n ($n = 12$–32) clusters are superparamagnetic at 93 K, with magnetic moments ranging from 0.35 to 1.09 μ_B/atom. A series of theoretical investigations of small Rh clusters had been conducted over the past two decades. Reddy et al. [3] calculated the stability and magnetic moments of Rh_n ($n = 2$–13) clusters using a combination of molecular dynamics and ab initio density-functional theory (DFT), and they found that the magnetic character and the magnetic moment per atom vary nonmonotonically with size. Bae et al. [6] investigated the structural and magnetic properties of Rh_n($n = 8$–64) clusters and found the simple cubic structure to be most favorable for up to $n - 27$. In addition, the magnetic moments in the low coordination simple cubic isomers agree closely with the observed values, thus explaining the origin of a long-standing experimental result. Recently, Soltani and Boudjahem [10] reported that the magnetic moments of Rh_n clusters are strongly related to the geometries and the spin states and that the calculated values of magnetism for the most stable clusters range from 0.67 to 2 μ_B/atom. Furthermore, the magnetic moments of these clusters are attributed mainly to the contribution of the $4d$ orbital.

Magnetism modulation of rhodium clusters is another important aspect for actual applications, and doping with another metal atom can be applied to modify the chemical and physical properties of pure rhodium clusters. Rhodium clusters doped with other transition-metal atoms can come into being distinctive structures and interesting properties. Manganese exhibits a distinguished magnetism property due to its half-filled $3d$ orbital. Small clusters of Mn are ferromagnetic, whereas the coupling between Mn atoms becomes ferrimagnetic with increasing size [15,16]. More interestingly, theoretical calculations [17] suggested that the magnetic enhancement of $Co_{n-1}Mn$ clusters is identified upon Mn substitution; this

[a] e-mail: lvjin_sxnu@163.com

Table 1. Calculated bond length d (Å), average binding energy per atom E_b (eV), magnetic moment M (μ_B) of the bare Mn_2 and Rh_2 cluster.

		Our work		Theoretical	Experimental
		PW91	PBE		
Mn_2	Bond length (Å)	2.600	2.616	2.600 [26,27]	3.17 [28]
	E_b (eV/atom)	0.492	0.441	0.49 [26,27]	0.44 ± 0.30 [29]
	μ (μB)	10	10	10 [26,27]	AFM [28]
Rh_2	Bond length (Å)	2.339	2.343	2.340 [6]	2.280 [30]
	E_b (eV/atom)	1.967	1.942	2.04 [8]	$1.46 + 0.11$ [30]
	μ (μB)	4	4	4 [6,8,12]	4 [30]

finding is consistent with the experimental result [18]. Similar magnetic enhancement is also found in Ni_nMn [19], Pd_nMn [20], and Au_nMn [21] clusters. Recently, Srivastava and Misra [22] studied small Rh_xMn_y ($x + y = 2$–4) clusters and found the ferromagnetic and ferrimagnetic alignments of atomic moments of Rh and Mn with the increase in the proportion of x and/or y. The magnetic moments of Rh range from 0.67 μ_B to 1.87 μ_B. Hang et al. [23] investigated the structures and relative stabilities of Rh_n clusters ($n = 2$–13) and binary Rh_mM (M = Fe, Co, Ni, and $m = 1$–6) clusters. They found that the growth mechanism of Rh_mM can be generated by attaching one M into the Rh_m host and that the Rh_mFe is a highly stable system. Nonetheless, to our knowledge, the magnetism evolution of Mn doped larger size rhodium clusters needs further investigation, and the influence of Mn atom on the magnetic behavior of rhodium clusters remains unclear.

The above findings brought about the following correlated questions regarding Mn doped Rh_n clusters: (1) How does Mn doping change the geometrical structures of Rh_n clusters? (2) Can the magnetic properties of pure Rh_n clusters be altered through the incorporation of Mn atom? We performed a systematic study on the geometry, relative stability, and magnetic properties of the Rh_{n+1} and Rh_nMn ($n = 1$–12) clusters using a DFT method. The main objectives of the present work are to identify the optimal doping site of Mn atom to Rh_n clusters and their magnetism coupling nature, to explore how the doped Mn atom impacts the magnetic behavior of Rh_n clusters, and to elucidate their magnetism origin. This paper is organized as follows. The details of the method are described in Section 2. The results and discussions are presented in Section 3, and the summary is presented in Section 4.

2 Computational methods

To search for the lowest-energy structures of Rh_{n+1} and Rh_nMn clusters, we considered a considerable amount of possible structural isomers for each size. Full geometry optimizations are performed using the spin-polarized DFT [24,25] in a $DMol^3$ package [26,27]. The electron density functional is treated by the generalized gradient approximation (GGA) with the PW91 exchange-correlation functional parameterized by Perdew et al. [28]. All electron calculations and the double-numerical basis with polarized (DNP) functions [29] were utilized in this work. For the numerical integration, a Medium quality mesh size was used, and the real space cutoff of the atomic orbital was set at 5.5 Å. The convergence criteria for structure optimization and energy calculations were set to Medium with the tolerance for density convergence in SCF, energy, gradient and displacement at 1×10^{-5} e/Å^3, 2.0×10^{-5} hartree, 1×10^{-5} a.u. and 0.005 Å, respectively. There are no imaginary frequencies for all the structures reported here, indicating that they are minimal on the potential energy surface. Additionally, considering the spin polarization, every geometry optimization has been carried out at various possible spin multiplicities. These two steps ensure that the obtained spin state is the most energetically preferred. Then, the net charge and the magnetic moments are evaluated by the Mulliken population analysis.

To check for the validity of the present computational scheme, we choose PW91 and PBE functions to perform some test calculations on Rh_2 and Mn_2 dimers. As listed in Table 1, the computed bond length, binding energy per atom (E_b) and magnetic moment (μ) results of PW91 functions for Rh_2 and Mn_2 clusters entirely agree well with previous theoretical [3,5,9,30] and experimental data [31–33]. The E_b of Rh_2 calculated to be 1.967 eV/atom has some difference with corresponding experimental values of $1.46 + 0.11$ eV/atom [33], while this value is consistent with previous theoretical results [5]. This indicates that our approach and accuracy are enough to describe the structures and properties of Rh_{n+1} and Rh_nMn clusters.

3 Results and discussion

3.1 Equilibrium geometries

The ground state structure and two low-lying isomers for each Rh_nMn cluster are displayed in Figures 1 and 2, together with the symmetries, magnetic moment, and energy relative (ΔE). Meanwhile, to examine the effects of dopant Mn on rhodium clusters, geometry optimizations of Rh_{n+1} ($n = 1-12$) clusters have been carried out using identical method and basis set. The lowest energy structures of pure Rh_{n+1} cluster are also displayed in Figures 1 and 2. For Rh_nMn ($n = 1-12$) clusters, about 450 initial configurations were optimized and many isomers have been obtained. We only include the isomers within 0.3 eV of the most stable structure.

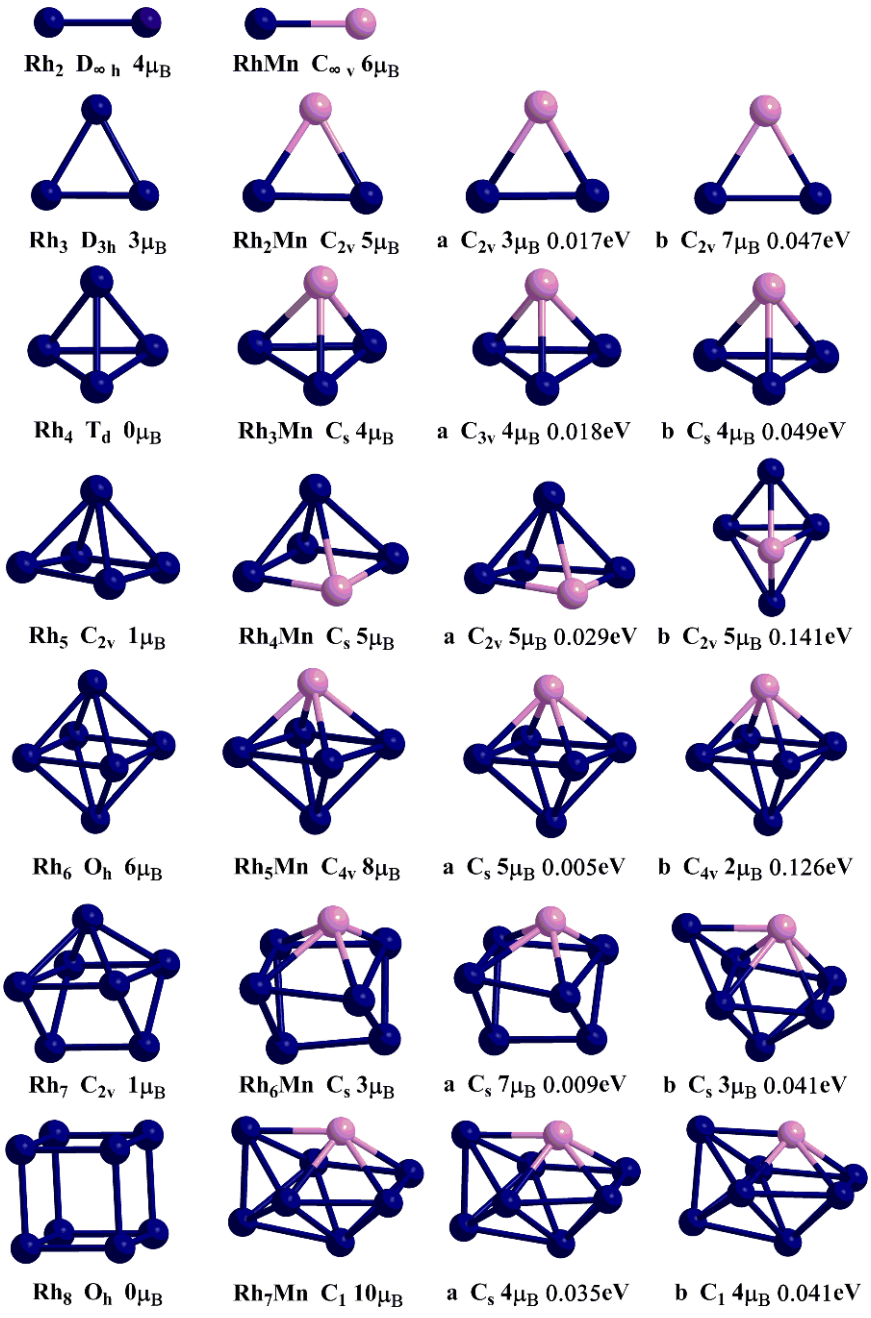

Fig. 1. Lowest-energy structures and low-lying isomers with relative energies (in eV) of Rh_nMn ($n = 1$–7) clusters. The ground state geometries of the corresponding bare Rh_n clusters are also given on the left. The blue and pink balls represent Rh and Mn respectively.

The bond length and the binding energy of RhMn are 2.305 Å and 1.742 eV/atom, respectively, which lies between that of Rh_2 (2.339 Å, 1.967 eV/atom) and Mn_2 (2.600 Å, 0.492 eV/atom). Compared with pure Rh_2 ($4\,\mu_B$), the magnetic moment of the RhMn dimer is increased by $2\,\mu_B$. The lowest energy structure of the Rh_3 cluster is an equilateral triangle (D_{3h}), which is consistent with the previous calculated results [10,34,35]. For Rh_2Mn, the most stable structure is an isosceles triangle (C_{2v}) with the Mn atom located at the apex, in which the Rh–Rh distance (2.569 Å) is 0.23 Å longer than that of the Rh_2 dimer. This structure has a total magnetic moment of $5\,\mu_B$.

Rh_4 is the smallest cluster that could assume a three dimensional structure. Our results show that the ground state of Rh_4 is a tetrahedron structure (T_d) with $0\,\mu_B$ of total magnetism, which is in good agreement with the theoretical results of Reddy et al. [3] and Aguilera-Granja [4]. The replacement of one Rh with Mn leads to a more distorted tetrahedron of Rh_3Mn (C_s) with the Mn atom

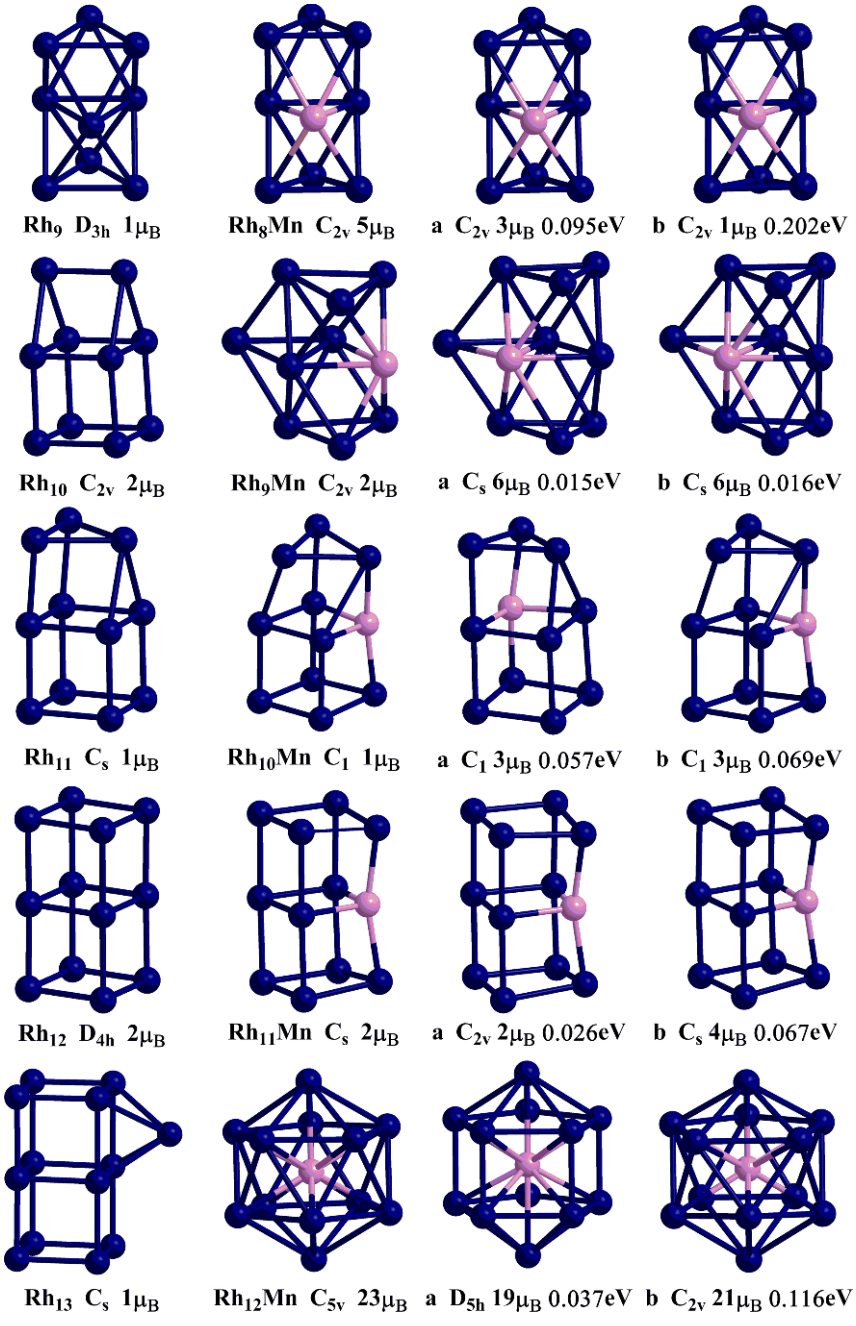

Fig. 2. Lowest-energy structures and low-lying isomers with relative energies (in eV) of Rh_nMn ($n = 8$–12) clusters. The ground state geometries of the corresponding bare Rh_n clusters are also given on the left. The blue and pink balls represent Rh and Mn respectively.

located at the apex and an evidently increased magnetism ($4\,\mu_B$). In contrast, the other two stable isomers lie above the lowest-energy structure by 0.018 eV and 0.049 eV in energy, respectively.

For Rh_5 cluster, the lowest-energy configuration is a square pyramidal structure with C_{2v} symmetry. Similar geometry has been reported by Reddy et al. [3] and Soltani and Boudjahem [10] as the ground state structure. Similar to the configuration of ground state Rh_5 cluster, the distorted square pyramidal (C_s) with the Mn atom at the square position is the most stable structure of Rh_4Mn clusters. It has a $5\,\mu_B$ total magnetic moment. The second lowest energy structure (C_s), which shares the same geometric structure with the lowest-energy of Rh_4Mn, is less favorable in energy by 0.002 eV. The third stable isomer is a triangular bipyramid (C_{2v}) with Mn atom lain at the middle plane and is 0.029 eV less stable in energy than the lowest energy structure.

The ground state Rh_6 adopts an octahedron with perfect O_h symmetry, which agrees well with the early studies [9,10,35]. In terms of Rh_5Mn, it is a nearly degenerate octahedron with Mn atom in vertex (C_s) with $8\,\mu_B$

magnetic moment. The other two lowest energy structures have the similar geometry but the different reduced magnetic moment ($5\,\mu_B$, $2\,\mu_B$) and lie 0.05 eV and 0.126 eV higher in energy with respect to the ground state.

The square capped prism with C_{2v} symmetry is the lowest energy structure of Rh_7 cluster, which is obtained as the ground state in references [5,7,9,10]. The lowest energy structure of Rh_6Mn is still derived from the Rh_7, namely, a square capped prism (C_s) with $3\,\mu_B$ magnetic moment, in which the Mn atom is located at the vertex position. The metastable state is also a square capped prism (C_s), and is only 0.003 eV higher in energy than the ground state. In contrast, the second lowest energy structure is a distorted capped octahedron with the impurity Mn atom at the vertex, and is energetically less favorable than the most stable structure by 0.009 eV.

As for the Rh_7Mn and Rh_9Mn clusters, their structures are clearly different from corresponding pure Rh_{n+1} clusters. The most stable structure of Rh_8 is a perfect cubic geometry (O_h). Our calculated minimum energy structure is in agreement with those reported in the literatures [5–7,9]. However, Rh_8 cluster is found to have a nonmagnetic ground state, possessing $0\,\mu_B$ magnetic moment, which was also obtained by Lv et al. [36]. While a bicapped octahedron (C_1) with Mn atom at the vertex position of the octahedron is the most stable structure of Rh_7Mn. It has $10\,\mu_B$ total magnetic moment, and is energetically lower than the metastable state ($4\,\mu_B$) by 0.035 eV. The other isomer similar to the Rh_7Mn with C_1 symmetry is 0.041 eV less stable than the lowest energy structure. For Rh_{10}, the lowest-energy structure can be viewed as a combination of one cube and one trigonal prism, which is in accordance with previous reports [7,9,10]. With regard to Rh_9Mn cluster, the most stable structure can be regarded as the derivatives of a double trigonal antiprismatic Rh_8Mn cluster with the Mn atom located at the middle triangle. The lowest-energy Rh_{10} and Rh_9Mn share equal total magnetic moment ($2\,\mu_B$). The next stable isomer has the same geometric configuration with the lowest-energy structure but has different magnetic moment ($6\,\mu_B$) and the energy difference between them is only 0.015 eV.

With regard to Rh_9 cluster, a double trigonal anti-prism (D_{3h}) with $1\,\mu_B$ total magnetic moment is the ground-state structure, which was obtained as the metastable structure by Futschek et al. [34]. Among the Rh_8Mn isomers, the lowest energy structure is the distorted double trigonal anti-prism with C_{2v} symmetry and the Mn atom located at the middle triangle. It has a total magnetic moment of $5\,\mu_B$. The second and third isomers are completely uniform in structure, and notable instability (0.095 and 0.202 eV, respectively).

For Rh_{11} cluster, we find a cubic structure with three atoms capping a face of Rh_8 as the minimum energy structure. Similar ground state structure has been reported by Bae et al. [6] and Aguilera-Granja et al. [7]. In the case of $Rh_{10}Mn$ clusters, the most stable structure is similar to that of the Rh_{11} clusters, and the Mn atom is located at the middle square. It has the same total magnetic moment ($1\,\mu_B$), and is energetically lower than the metastable state with same magnetism by 0.008 eV. As seen in Figure 2, the third lowest energy structure has the same geometry as the ground state, and lies 0.057 eV higher in energy.

A combination of two cubic structures with D_{4h} symmetry is the lowest energy structure for Rh_{12} cluster, which is in accordance with previous results for rhodium cluster [6,7,9,10]. For $Rh_{11}Mn$ cluster, the most stable structure shows a similar structure to that of the ground state Rh_{12} cluster and the Mn atom located at the middle square. It has the same structure and total magnetic moment ($2\,\mu_B$), and is energetically lower than the metastable state by 0.009 eV and 0.026 eV respectively.

With regard to Rh_{13} cluster, capping of a side face of Rh_{12} is favored with $1\mu B$ magnetic moment. This is the best agreement with the value obtained by Sun et al. [37,38] among all the theoretical results obtained so far. For $Rh_{12}Mn$ cluster, we considered a lot of initial geometries including the icosahedra (I_h), cuboctahedral (O_h), anti-cuboctahedral (D_{3h}), bilayer hcp (C_{3v}), buckled biplanar (C_{2v}), decahedral (D_{5h}) and capping of a side face of two cubic structures et al. in this paper. The most stable structure of $Rh_{12}Mn$ is the icosahedra structure (C_{5v}) with Mn atom at the center, and the coupling among all atoms is ferromagnetic. The total magnetic moment is $23\,\mu_B$. The next two stable isomers are found to be a decahedral structure (D_{5h}) (a) and a distorted icosahedra structure (C_{2v}) (b). Their energies are only 0.037 and 0.116 eV above the ground state, respectively. However, the energy of cubic structures with Mn atom capping of a side face is 0.798 eV above the ground state.

The overall structural evolutionary trend shows that, except $n = 7$, 9 and 12, the Mn substitution doping almost does not bring much influence on the primary configurations, and the ground state structure of Rh_nMn is still similar to that of the corresponding pure ones. Additionally, the Mn atom can be looked upon as a substitution impurity in the pure Rh_{n+1} cluster. A bicapped octahedron (C_1) with Mn atom at the vertex position of the octahedron is the most stable structure of Rh_7Mn cluster. The Rh_9Mn cluster is geometrically reconstructed and adopts the double trigonal antiprismatic with Mn atom located at the middle triangle. The most stable structure of $Rh_{12}Mn$ is the icosahedra structure (C_{5v}) with Mn atom at the center.

3.2 Relative stability

In order to study the stability of Rh_nMn clusters, we plot the binding energy per atom (E_b) of the lowest energy structures as a function of cluster size n for both Rh_{n+1} and Rh_nMn clusters (n = 1–12), as shown in Figure 3a. The atomic average binding energy $E_b(n)$ can be expressed by the following formulas:

$$E_b(\mathrm{Rh}_n\mathrm{Mn}) = \frac{nE(\mathrm{Rh}) + E(\mathrm{Mn}) - E(\mathrm{Rh}_n\mathrm{Mn})}{n+1} \quad (1)$$

$$E_b(\mathrm{Rh}_{n+1}) = \frac{(n+1)E(\mathrm{Rh}) - E(\mathrm{Rh}_{n+1})}{n+1} \quad (2)$$

where E is the total energy of the respective atoms or clusters. The average binding energy of Rh_nMn clusters increases monotonically with size which indicates that

these clusters can continuously gain energy during the growth process. A similar trend is also observed in Rh_{n+1} clusters. As shown in Figure 3a, in the initial stage ($n = 1$–8) E_b increases speedily, when n goes from 9 to 12, the E_b increases gradually and exhibits obvious convergence trend. Meanwhile, for the Rh_nMn and Rh_{n+1} clusters of the same size, the E_b decreases with the substitution of one Rh atom by one Mn atom. Therefore, it is clear that the Mn-doping can weaken the energetic stability of Rh clusters. Similar phenomena that the binding energy per atom decreases with the substitution of Mn atom also appeared in the previous studies [17,19]. This decrease mainly stems from that the cohesive energy of bulk Rh (5.75 eV) is significantly larger than that of bulk Mn (2.92 eV) [39], indicating that the stability of pure Rh_{n+1} clusters is weakened by replacing one Rh atom with one Mn atom. The tendency of average binding energy of our calculated dimers is Rh_2 (1.967 eV) > RhMn (1.742 eV) > Mn_2 (0.492 eV), in agreement with the above analysis based on the cohesive energy of bulk. In order to have a further look into the stability behavior of the size-dependent Rh_{n+1} and Rh_nMn ($n = 1$–12) clusters, the fragmentation energy $\Delta_1E(n)$ and the second-order difference energy $\Delta_2E(n)$ are calculated using the following formulas:

$$\Delta_1E(\mathrm{Rh}_{n+1}) = E(\mathrm{Rh}_n) + E(\mathrm{Rh}) - E(\mathrm{Rh}_{n+1}) \quad (3)$$

$$\Delta_2E(\mathrm{Rh}_{n+1}) = E(\mathrm{Rh}_{n+2}) + E(\mathrm{Rh}_n) - 2E(\mathrm{Rh}_{n+1}) \quad (4)$$

$$\Delta_1E(\mathrm{Rh}_n\mathrm{Mn}) = E(\mathrm{Rh}_{n-1}\mathrm{Mn}) + E(\mathrm{Rh}) - E(\mathrm{Rh}_n\mathrm{Mn}) \quad (5)$$

$$\Delta_2E(\mathrm{Rh}_n\mathrm{Mn}) = E(\mathrm{Rh}_{n+1}\mathrm{Mn}) + E(\mathrm{Rh}_{n-1}\mathrm{Mn}) - 2E(\mathrm{Rh}_n\mathrm{Mn}) \quad (6)$$

where $E(\cdot)$ is the total energy of respective atoms or clusters. Based on the above formulas, the evolution of $\Delta_1E(n)$ and $\Delta_2E(n)$ is plotted in Figures 3b and 3c, respectively. From the graph, it is observed that both curves of $\Delta_1E(n)$ and $\Delta_2E(n)$ show an interesting pronounced even–odd oscillatory behavior at $n \leq 8$, indicating that the Rh_{n+1} and Rh_nMn clusters with even number of atoms are relatively more stable than their neighboring sizes. This can be explained through the electron pairing effect [40,41]. It is generally known that the Rh and Mn atoms all have an odd number of valence electrons, leading to the clusters with even number of atoms fully share electrons. Therefore, the Rh_{n+1} and Rh_nMn clusters with even number of atoms are more stable than those with odd number of atoms. For the doped clusters, the curves of $\Delta_1E(n)$ and $\Delta_2E(n)$ share identical peaks at $n = 3$, 5, 8 and 11. That is to say, Rh_3Mn, Rh_5Mn, Rh_8Mn and $Rh_{11}Mn$ are more stable than their neighbors. In addition, the relative stability of $n = 3$, 5, 7 and 11 for Rh_{n+1} clusters is also reported in previous studies [10].

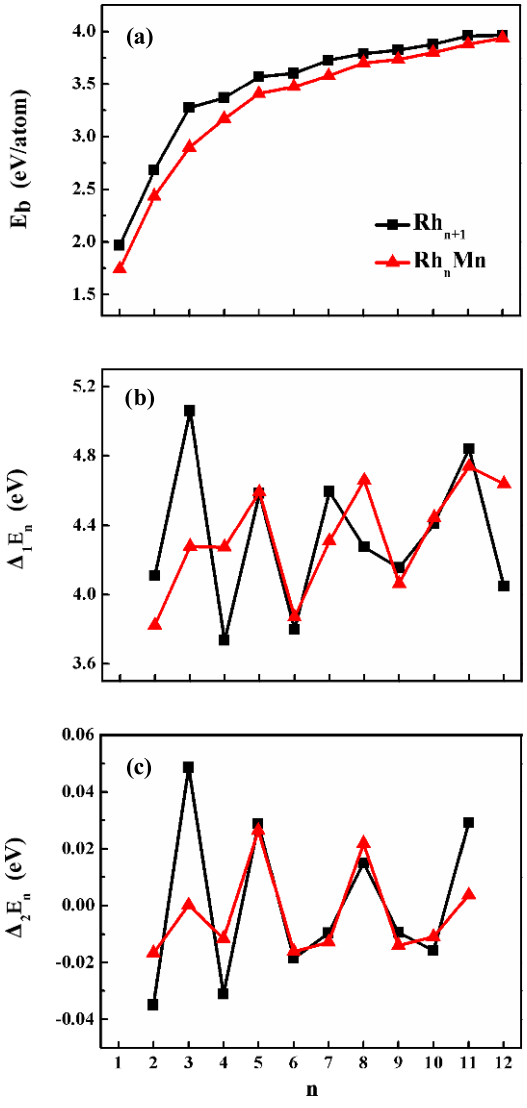

Fig. 3. Size dependence of averaged atomic binding energies (a), fragmentation energies (b), and second-order difference energies (c), for the lowest energy structures of Rh_{n+1} and Rh_nMn ($n = 1$–12) clusters.

The magnetic stability of these clusters can be investigated by examining the spin gaps as a function of the cluster size. The spin gaps for a magnetic cluster are defined as follows:

$$\delta_1 = -(\varepsilon_{\mathrm{HOMO}}^{\mathrm{majority}} - \varepsilon_{\mathrm{LUMO}}^{\mathrm{min\,ority}}) \quad (7)$$

$$\delta_2 = -(\varepsilon_{\mathrm{HOMO}}^{\mathrm{min\,ority}} - \varepsilon_{\mathrm{LUMO}}^{\mathrm{majority}}). \quad (8)$$

Commonly a given spin arrangement is classified as magnetically stable if both δ_1 and δ_2 are positive. Namely, the LUMO of the minority spin lies above the HOMO of the majority spin and vice versa. These represent the

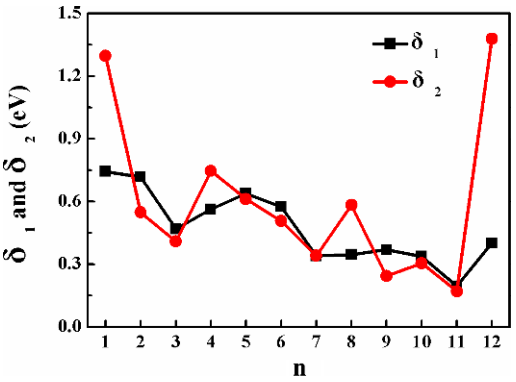

Fig. 4. Size dependence of the spin gaps of Rh_{n+1} and Rh_nMn ($n = 1$–12) clusters.

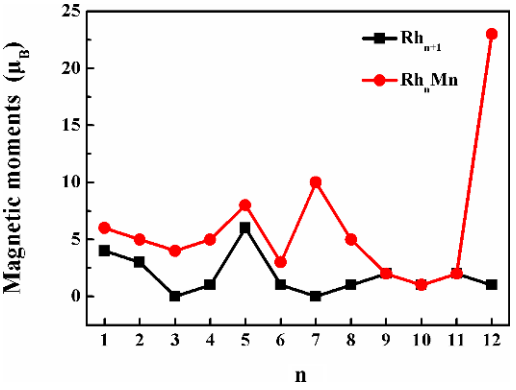

Fig. 5. Size dependence of the magnetic moments for Rh_{n+1} and Rh_nMn ($n = 1$–12) clusters.

energy required to move an infinitesimal amount of charge from the HOMO of one spin channel to the LUMO of the other. So magnitude of spin gaps is a measure of chemical activeness of clusters [42]. The higher the spin gap, the more stable the cluster. The spin gaps (δ_1 and δ_2) of Rh_{n+1} and Rh_nMn clusters are described in Figure 4. One can clearly see that both δ_1 and δ_2 are positive for all the Rh_{n+1} and Rh_nMn clusters, and have a generally decreasing trend with the increase of cluster size. The higher spin gaps of the small size clusters probably stems from the quantum size effect [43].

3.3 Magnetic properties

The total magnetic moment of Rh_nMn ($n = 1$–12) clusters is calculated and presented as a function of cluster size in Figure 5, where the values of the pure rhodium clusters are also plotted for comparison. For Rh_{n+1} clusters, our results of total magnetic moment partly accord with those reported in the literatures [3,4,7,8,34,38]. After doping Mn, most of the Rh clusters have an enhanced total magnetic moment, except for $n = 9$–11. In detail, for $n = 1$, 2, 5, 6, the total magnetic moment of Rh_nMn clusters is enhanced by 2 μ_B; for $n = 3$, 4, 8, the total magnetic moment is enhanced by 4 μ_B; while for $n = 7$ and 12, the total magnetic moment is greatly increased by 10 μ_B and 22 μ_B respectively. Moreover, the calculated data of the

Table 2. The average magnetic moment of Rh atom (M_1, units of μ_B) for Rh_{n+1}clusters, the Mn atom (M_2, units of μ_B) and the average magnetic moments of Rh atom (M_3, units of μ_B) and for Rh_nMn clusters.

n	M_1	M_2	M_3	n	M_1	M_2	M_3
1	2.00	4.74	1.26	7	0.00	4.253	0.82
2	1.00	4.17	0.41	8	0.11	4.448	0.07
3	0.00	4.35	−0.12	9	0.20	−4.15	0.68
4	0.20	4.49	0.13	10	0.09	2.70	−0.17
5	1.00	4.311	0.73	11	0.17	2.27	−0.03
6	0.14	4.152	−0.19	12	0.08	3.788	1.60

average magnetic moments of Rh and Mn atoms in Rh_{n+1} and Rh_nMn clusters are shown in Table 2. It is clearly seen that the average magnetic moment of Rh atoms lies in the range (0.03–1.60 μ_B) as the cluster size increasing, which is much smaller than that of Mn atom (2.27–4.49 μ_B) in Rh_nMn clusters. This implies that the increase of total magnetic moments of these clusters mainly comes from the doping Mn atom. Additionally, from Table 2, we can conclude that the oscillating magnetic behavior of Rh_nMn clusters is consistent with the variation of the average magnetic moment of Rh atoms, which is influenced by the doping Mn atom.

We systematically investigate the local moments of clusters and the detailed data is listed in Figure 6. For $n = 1$, 2, 5, 7, 8 and 12 clusters, the Rh–Mn and Rh–Rh magnetic interaction all exhibit ferromagnetic coupling, and they acquire the larger total magnetic moments of 6 μ_B, 5 μ_B, 8 μ_B, 10 μ_B, 5 μ_B and 23 μ_B respectively. Among them, the local magnetic moments of Mn and Rh atoms in the $Rh_{12}Mn$ cluster are significantly larger, causing the largest magnetic moment of 23 μ_B. While for $n = 3$, 10 and 11, the Rh–Mn and Rh–Rh moments all present antiferromagnetic coupling, and finally, the total magnetism of them is remarkably small and the magnetism are 4 μ_B, 1 μ_B and 2 μ_B respectively. Among them, total magnetic moment of $Rh_{10}Mn$ and $Rh_{11}Mn$ clusters remains unchanged compared with the pure Rh cluster. For $n = 4$, the doped Mn atom exhibits ferromagnetic alignment with adjacent Rh atoms, but Rh–Rh is coupled antiferromagnetically, and finally obtains the magnetic moments of 5 μ_B. For Rh_6Mn cluster, the Mn atom shows antiferromagnetic alignment with adjacent Rh atoms, but the Rh atoms are all ferromagnetic, and finally obtains the magnetic moments of 3 μ_B. As same as the magnetic order of Rh_6Mn cluster, the magnetism of Rh_9Mn cluster is 2 μ_B. In addition, the Mn atom provides the antiferromagnetism and yields 4.15 μ_B local magnetic moment only in Rh_9Mn cluster in the present work. This could be a reason for the unchanged total magnetic moment of Rh_9Mn clusters. As discussed above, the magnetic coupling between Mn–Mn and Mn–TM atoms is one of the important reasons for the variation of the magnetism.

Meanwhile, the local magnetic moments of Rh atoms in Rh_nMn clusters are significantly decreased compared to the pure Rh clusters, and the number of antiferromagnetic coupling increases. The total magnetic moments of Rh_nMn clusters primarily stem from the Mn atom and the

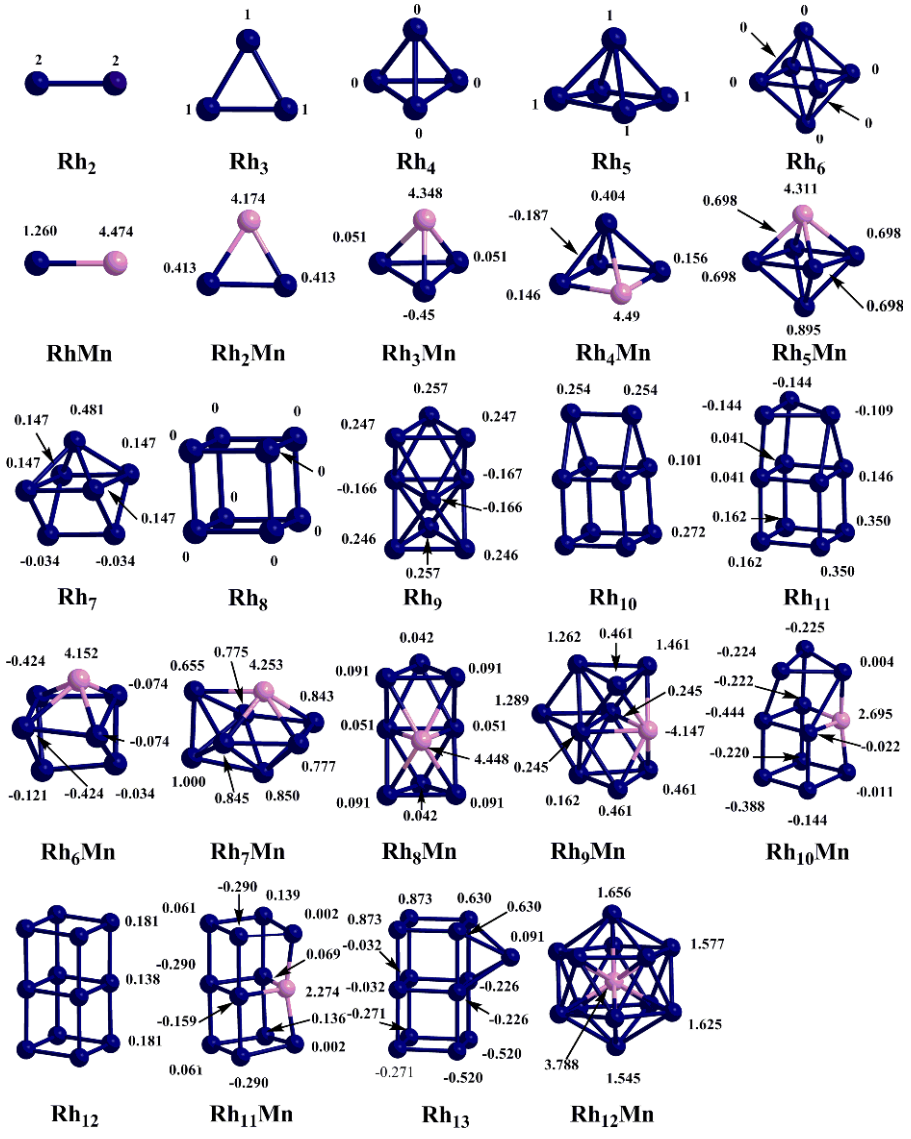

Fig. 6. The local magnetic moments of the ground-state structures of Rh_{n+1} and Rh_nMn ($n = 1$–12) clusters.

Table 3. The average bond lengths (L_0) for Rh_{n+1} clusters, Rh–Rh (L_1) and Rh–Mn atoms (L_2) for Rh_nMn clusters.

n	L_0/Å	L_1/Å	L_2/Å	n	L_0/Å	L_1/Å	L_2/Å
1	2.341	–	2.305	7	2.488	2.684	2.535
2	2.454	2.569	2.298	8	2.589	2.598	2.614
3	2.516	2.583	2.417	9	2.495	2.645	2.551
4	2.534	2.555	2.465	10	2.504	2.539	2.3
5	2.606	2.622	2.485	11	2.477	2.489	2.287
6	2.64	2.683	2.434	12	2.513	2.743	2.607

local magnetic moment of Mn atom almost maintains the atomic magnetic moment ($5\,\mu_B$). It is chiefly because the Mn atom presents the fantastic magnetic properties due to the particular electronic configuration $3d^5 4s^2$. Abundant experimental measurements in combination with theoretical calculations have commonly confirmed that small Mn_n clusters exhibit ferromagnetic coupling with a magnetic moment of $5\,\mu_B$ per atom, whereas the coupling between Mn atoms becomes ferrimagnetic as the size increasing [44,45]. This illustrates that the antiferromagnetic coupling is increased in Rh clusters after doping a Mn atom. Additionally, the local magnetic moment of Mn atom approximately keeps the atomic magnetic moment and finally leads to the greater magnetic moment of Rh_nMn clusters. However, the local magnetic moment of Mn atom for $Rh_{10}Mn$ and $Rh_{11}Mn$ clusters is $2.695\,\mu_B$ and $2.274\,\mu_B$ respectively. This could be owing to the ground state structure of $Rh_{10}Mn$ and $Rh_{11}Mn$ which remain as the cubic structures. Previous work by Bae et al. [6] supported the finding that the cubic structures have lower magnetic moments than the dense packed icosahedra isomers, which agree closely with the experiments. Hence, the cubic structure is probably one reason that the total magnetic moment of $Rh_{10}Mn$ and $Rh_{11}Mn$ clusters remains unchanged. Noteworthy, Rh_8 cluster is found to have a

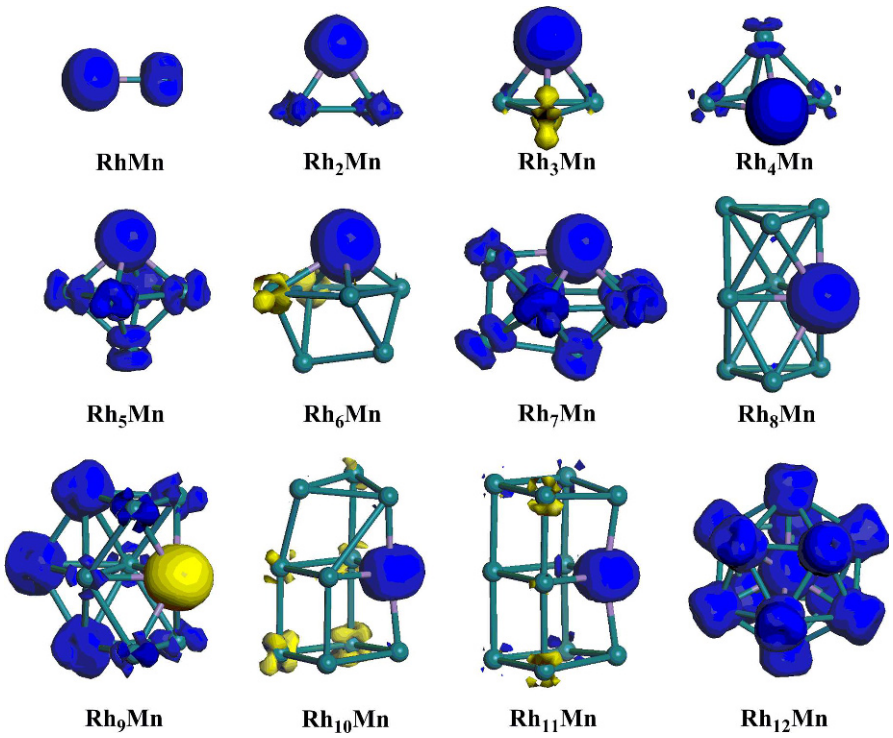

Fig. 7. The spin density of Rh_nMn ($n = 1$–12) clusters. (The isosurface value is 0.15 a.u.)

perfect cubic geometry, possessing 0 μ_B magnetic moment. However, the magnetic moment of Rh_7Mn is increased to 10 μ_B. The principal reason is that the ground state structure of Rh_7Mn cluster is a bicapped octahedron rather than the cubic geometry.

In order to explore the magnetic behavior of Rh_nMn clusters, we now analyze the origin of such oscillating magnetic behavior of Rh_nMn clusters. In Table 3, we have listed the average bond lengths (L_0) for Rh_{n+1} clusters, Rh–Rh (L_1) and Rh–Mn atoms (L_2) for Rh_nMn clusters at their stable structures. It is clearly seen that the bond length of L_1 is larger than that of L_0 and the increased value varied from 0.009 Å to 0.23 Å, implying doping Mn atoms tend to weaken the hybridization in host Rh atoms, which should play a crucial role for the enhancement of the magnetism. Generally, for the long interatomic distance, d electron localization and the low hybridization with s states lead to the weak interaction, and finally generate a ferromagnetic alignment [17,46]. This means that a large distance indicates a weak bonding between Rh–Rh atoms and forms more ferromagnetic coupling, resulting in relatively larger magnetic moments for Rh_nMn clusters. From Tables 2 and 3, we notice that the average Rh–Rh and Rh–Mn bond lengths of $Rh_{12}Mn$ are quite long, corresponding to the largest total magnetic moment of 23 μ_B. Similar behavior is also observed in Rh_7Mn cluster with total magnetic moment of 10 μ_B, which possesses the relatively long average Rh–Rh bond length. The value of 2.683 Å for Rh_6Mn cluster is the third longest L_1, while it acquires a smaller magnetic moment of 3 μ_B. It could be attributed to the smaller Rh–Mn bond length in Rh_6Mn cluster, which brings about the antiferromagnetic coupling between Rh–Mn atoms. It implies that the magnetic moment of Rh_nMn clusters is very sensitive to the Rh–Mn bond length. In fact, the very short Rh–Mn bond in the Rh_6Mn cluster is inclined to cause much stronger d-d interaction. As a consequence, the Mn atom tends to be antiferromagnetically coupled to Rh atoms (as seen in Tab. 2) and further decreases the total magnetic moment. Such antiferromagnetic alignment also appears for other size of Rh_nMn clusters ($n = 3$, 9, 10, 11). Therefore, the total magnetic moment of Rh_9Mn, $Rh_{10}Mn$ and $Rh_{11}Mn$ clusters is very small and even remains unchanged compared with that of the pure Rh_n cluster, owing to the rather smaller average Rh–Rh and Rh–Mn bond length.

To gain more insight into the magnetism of the Rh_nMn clusters, we explored the spin densities of these alloy clusters. In Figure 7, we plotted the difference between the charge density for up-spin and down-spin electrons. As can be seen, the contributions to magnetism of the cluster mainly originate from Mn atom in Rh_nMn and the Rh atoms have little influence on it. And the distribution of the spin densities around the Mn atom is apparently larger than other Rh atoms, implying that Mn atom possesses relatively larger magnetic moments. Additionally, it can be clearly seen that the rhodium host atoms all present antiferromagnetic coupling with the doped Mn atom in the Rh_9Mn cluster, while between the Rh host atoms, the magnetism odering is ferromagnetic, leading to its magnetic moment retaining unchange. Besides, the local spin moments of Rh atoms are found to align ferromagnetically with other Rh and Mn atoms in Rh_5Mn, Rh_7Mn and $Rh_{12}Mn$ clusters (see Fig. 7), leading to the relatively larger total magnetic moments than other clusters.

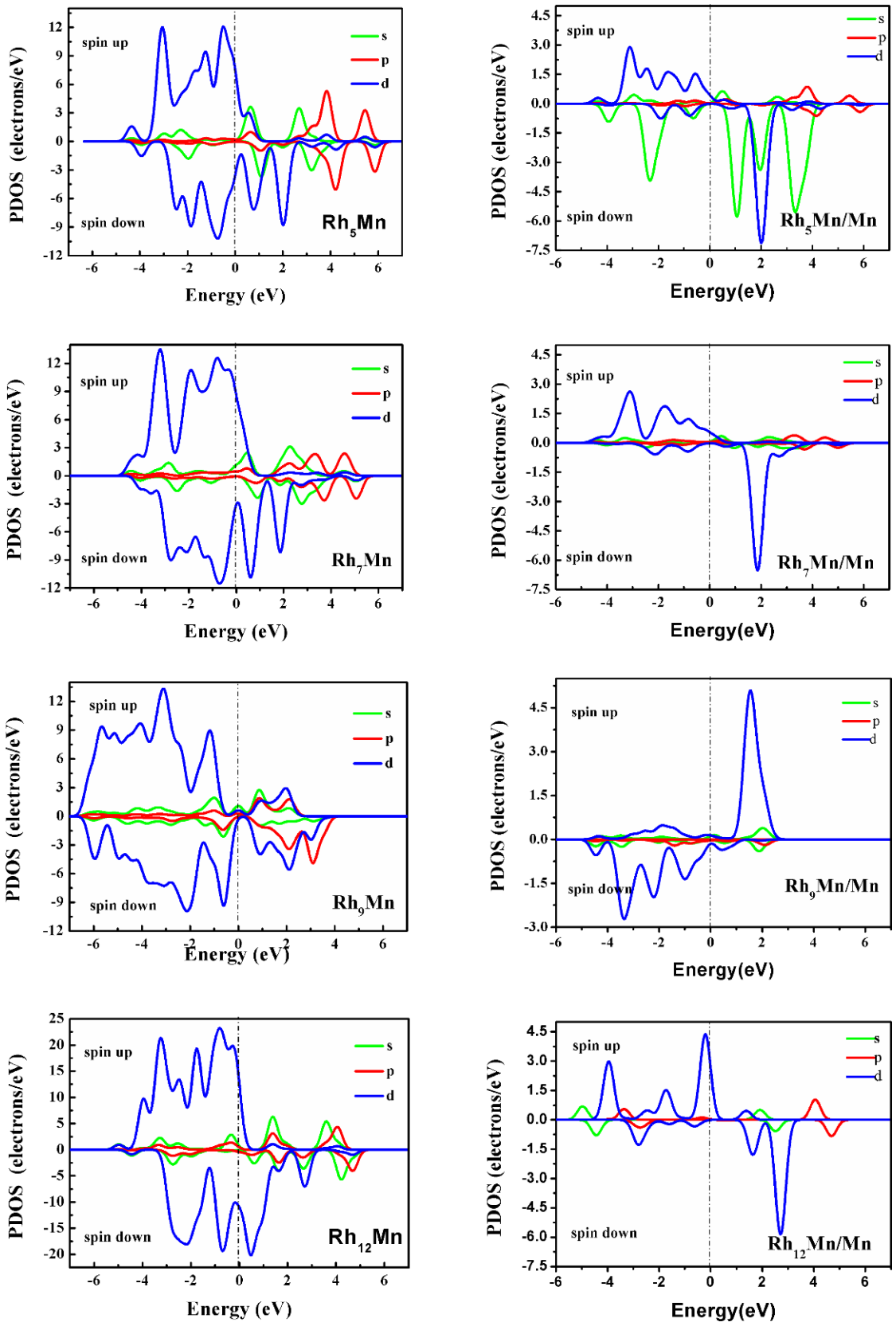

Fig. 8. The calculated PDOS of the Rh_nMn ($n = 5$, 7, 9, 12) clusters and Mn atom in these clusters. The dashed line refers to the Fermi level which is shifted to zero.

To obtain a deeper insight into the magnetism of the Rh_nMn alloy clusters, it is essential to analyze the *s*-, *p*-, and *d*-projected partial densities of states (PDOS) of Rh_nMn clusters. As shown in Figure 8, the Rh_5Mn, Rh_7Mn, Rh_9Mn and $Rh_{12}Mn$ clusters are taken as examples to explore the magnetic behavior. Spin-down density is plotted as negative, and the dashed line refers to the Fermi level which is shifted to zero. Clearly, the d states of both Rh host atoms and doping Mn atoms in Rh_nMn clusters have a dominant contribution to the magnetic behavior compared to the *sp* states. This result is consistent with the previous analysis results. In general, the relative shift between the spin-up and spin-down bands can indicate the degree of spin exchange splitting, moreover, the larger the spin exchange splitting of DOS, the larger the magnetic moment of cluster [47]. As shown in Figure 8, the Rh_nMn ($n=5$, 7, 9, 12) clusters exhibit varying degrees of spin exchange splitting. The *d* electrons of $Rh_{12}Mn$ cluster show the largest spin exchange splitting, next is the Rh_5Mn and Rh_7Mn, and the Rh_9Mn cluster has the smallest spin exchange splitting. This is just consistent with the calculation results of their total magnetic moment ($Rh_{12}Mn/23\,\mu_B$, $Rh_5Mn/8\,\mu_B$, $Rh_7Mn/10\,\mu_B$ and $Rh_9Mn/2\,\mu_B$, respectively). Meantime, the PDOSs of these clusters present strong asymmetry below the Fermi level, which also cause them obtained larger magnetism. For the PDOS of the Rh_5Mn and Rh_7Mn, the *d*-projected PDOS of Mn atom is rather localized, and the majority spin is almost fully occupied. Consequently, the Mn atom of Rh_5Mn and Rh_7Mn possesses magnetic moment of $4.311\,\mu_B$ and $4.253\,\mu_B$, respectively. However, in the case of Rh_9Mn cluster, the DOS for spin-up and spin-down states almost simultaneously appear in the same eigenvalue of energy, which indicates that there is almost no exchange splitting. Meanwhile, the spin-down *d* electrons integral area of Mn atom in the Rh_9Mn is larger than that of spin-up below the Fermi level, which suggests that the local magnetic moment of Mn atom is a negative value. Finally both effects make the magnetism of Rh_9Mn remain unchanged with Mn doping. For $Rh_{12}Mn$ cluster, the d electrons peak of spin-up and spin-down is broadened around 24.3 and −20.0 eV below the Fermi level respectively, as a result, obtaining the largest magnetic moment of $23\,\mu_B$.

4 Conclusion

Using density functional DFT/GGA/PW91 method, we have discussed the structure, stability and magnetic properties of Rh_{n+1} and Rh_nMn clusters for $n=1$–12. The ground state structures of Rh_nMn ($n=1$–6, 8, 10, 11) clusters are analogous to those of the corresponding pure Rh_{n+1} cluster, and the Mn atom can be looked upon as a substitutional impurity. The Rh_nMn ($n=7,9,12$) clusters occurs substantially geometry reconstruction. The most stable structures of Rh_7Mn and Rh_9Mn clusters are a bicapped octahedron (C_1) with Mn atom at the vertex position of the octahedron and a double trigonal antiprismatic with Mn atom located at the middle triangle respectively. The most stable structure of $Rh_{12}Mn$ is the icosahedra structure (C_{5v}) with Mn atom at the center. Meanwhile, the E_b of Rh_nMn clusters is decreased with the substitution of one Rh atom by one Mn atom, indicating that the Mn-doping can weaken the energetic stability of Rh clusters. The calculated fragmentation energy and the second-order difference energy of the Rh_nMn ($n \leq 12$) clusters show the same odd–even alternation tendency with clusters size increasing. The stability analysis of entire Rh_nMn clusters indicates that the Rh_6Mn, Rh_9Mn and $Rh_{11}Mn$ clusters are more stable than their neighbors. Besides, both δ_1 and δ_2 are positive for all Rh_nMn clusters, demonstrating the magnetic stability of these clusters. Magnetism analysis shows that the doping of Mn atom increases the total magnetic moment of Rh_nMn clusters, except for the magnetic moment of Rh_9Mn, $Rh_{10}Mn$ and $Rh_{11}Mn$ remaining unchanged. Specifically, for $n=1$, 2, 5 and 6, the magnetic moment is increased by $2\,\mu_B$; for $n=3$, 4 and 8, the increased magnetic moment is $4\,\mu_B$; for $n=7$ and 12, the magnetic moment is increased to $10\,\mu_B$ and $23\,\mu_B$ respectively. This magnetic behavior can be attributed to the increase in Rh–Mn and Rh–Rh bond lengths, the different degrees of antiferromagnetic coupling between atoms and the particular cubic structures of Rh clusters.

This work was supported by the National Natural Science Foundation of China (Grant No. 21301112) and the Ph. D. Program Foundation of Ministry of China (Grant No. 20131404120001).

Author contribution statement

This paper origins from the coorperation of all authors. RS performed the primary calculation work and results analysis and wrote this manuscript. LS revised the manuscript. And JL contributed to the conception of this study and gave the guidance in theoretical explanation sections in this paper. HSW provides much valuable discussions in the writing process of original manuscript, much help in our study direction and in construction of our laboratory

References

1. A.J. Cox, J.G. Louderback, L.A. Bloomfield, Phys. Rev. Lett. **71**, 923 (1993)
2. A.J. Cox, J.G. Louderback, S.E. Aspeal, L.A. Bloomfield, Phys. Rev. B **49**, 12295 (1994)
3. B.V. Reddy, S.K. Nayak, S.N. Khanna, B.K. Rao, P. Jena, Phys. Rev. B **59**, 5214 (1999)
4. F. Aguilera-Granja, J.L. Rodríguez-López, K. Michaelian, E.O. Berlanga-Ramírez, A. Vega, Phys. Rev. B **66**, 224410 (2002)
5. Y.C. Bae, H. Osanai, V. Kumar, Y. Kawazoe, Phys. Rev. B **70**, 195413 (2004)
6. Y.C. Bae, V. Kumar, H. Osanai, Y. Kawazoe, Phys. Rev. B **72**, 125427 (2005)
7. F. Aguilera-Granja, L.C. Balbás, A. Vega, J. Phys. Chem. A **113**, 13483 (2009)
8. M.A. Mora, M.A. Mora-Ramírez, M.F. Rubio-Arroyo, Int. J. Quantum Chem. **110**, 2541 (2010)

9. J.L.F. Da Silva, M.J. Piotrowski, F. Aguilera-Granja, Phys. Rev. B **86**, 125430 (2012)
10. A. Soltani, A.G. Boudjahem, Comput. Theor. Chem. **1047**, 6 (2014)
11. X. Quek, Y. Guan, E.J. Hensen, Catal. Today **183**, 72 (2012)
12. C. Zhao, H. Wang, C. Xiao, X. Mu, P. Dyson, Y. Kou, J. Catal. **250**, 33 (2007)
13. J.A. Baeza, L. Calvo, M.A. Gilarranz, J.J. Rodriguez, Chem. Eng. J. **240**, 271 (2014)
14. D. Loffreda, D. Simon, P. Sautet, J. Chem. Phys. **108**, 6447 (1998)
15. C.A. Baumann, R.J. Van Zee, S.V. Bhat, W. Weltner Jr., J. Chem. Phys. **78**, 190 (1983)
16. M.B. Knickelbein, Phys. Rev. B **70**, 014424 (2004)
17. N.F. Shen, J.L. Wang, L.Y. Zhu, Chem. Phys. Lett. **467**, 114 (2008)
18. S.Y. Yin, R. Moro, X.S. Xu, W.A. de Heer, Phys. Rev. Lett. **98**, 113401 (2007)
19. B.R. Wang, H.Y. Han, Z. Xie, J. Mol. Struct. **1062**, 174 (2014)
20. Y.W. Mu, Y. Han, J.L. Wang, J.G. Wan, G.H. Wang, Phys. Rev. A **84**, 053201 (2011)
21. D. Die, X.Y. Kuang, J.J. Guo, B.X. Zheng, J. Phys. Chem. Solids **71**, 770 (2010)
22. A.K. Srivastava, N. Misra, Comput. Theor. Chem. **1047**, 1 (2014)
23. T.D. Hang, H.M. Hung, L.N. Thiem, Hue, M.T. Nguyen, Comput. Theor. Chem. **1068**, 30 (2015)
24. W. Kohn, L.J. Sham, Phys. Rev. B **140**, 1133 (1965)
25. R.G. Parr, W.T. Yang, *Density-functional theory of atoms and molecules* (Oxford University Press, Oxford, 1989)
26. B. Delley, J. Chem. Phys. **92**, 508 1990
27. B. Delley, J. Chem. Phys. **113**, 7756 (2000)
28. J.P. Perdew, J. Chevary, S.H. Vosko, K.A. Jackson, M.R. Pederson, D.J. Singh, C. Fiolhais, Phys. Rev. B **46**, 6671 (1992)
29. B. Delley, J. Chem. Phys. **92**, 508 (1990)
30. P. Bobadova-Parvanova, K.A. Jackson, S. Srinivas, M. Horoi, J. Chem. Phys. **122**, 14310 (2005)
31. K.D. Bier, T.L. Haslett, A.D. Kirkwood, M. Moskovits, J. Chem. Phys. **89**, 6 (1988)
32. M.D. Morse, Chem. Rev. **86**, 1049 (1986)
33. K.A. Gingerich, D.L. Cocke, J. Chem. Soc. Chem. Commun. **9**, 536 (1972)
34. T. Futschek, M. Marsman, J. Hafner, J. Phys.: Condens. Matter **17**, 5927 (2005)
35. M.R. Beltrán, F.B. Zamudio, V. Chauhan, P. Sen, H.P. Wang, Y.J. Ko, K. Bowen, Eur. Phys. J. D **67**, 63 (2013)
36. J. Lv, F.Q. Zhang, X.H. Xu, H.S. Wu, Chem. Phys. **363**, 65 (2009)
37. Y. Sun, M. Zhang, R. Fournier, Phys. Rev. B **77**, 075435 (2008)
38. Y. Sun, R. Fournier, M. Zhang, Phys. Rev. A **79**, 043202 (2009)
39. C. Kittel, *Introduction to solid state physics*, 8th edn. (Wiley, New York, 2005)
40. D. Die, X.Y. Kuang, B. Zhu, J.J. Guo, Physica B **406**, 3160 (2011)
41. M.A. Tafoughalt, M. Samah, Physica B **407**, 2014 (2012)
42. S. Datta, M. Kabir, T.S. Dasgupta, A. Mookerjee, Phys. Rev. B **80**, 085418 (2009)
43. N.S. Venkataramanan, R. Sahara, H. Mizuseki, Y. Kawazoe, J. Phys. Chem. A **114**, 5049 (2010)
44. T. Sondón, J. Guevara, A. Saul, Phys. Rev. B **75**, 104426 (2007)
45. C.A. Baumann, R.J. Van Zee, S.V. Bhat, W. Weltner Jr., J. Chem. Phys. **78**, 190 (1983)
46. J. Mejía-López, A.H. Romero, M.E. Garcia, J.L. Morán-López, Phys. Rev. B **78**, 134405 (2008)
47. G.W. Zhang, Y.P. Feng, C.K. Ong, Phys. Rev. B **54**, 17208 (1996)